ACTA SCIENTIARUM POLONORUM
Acta Sci. Pol. Technol. Aliment. 24(1) 2025, 47–65
www.food.actapol.net pISSN 1644-0730 eISSN 1898-9594 http://doi.org/10.17306/J.AFS.001268

ORIGINAL PAPER

Received: 13.08.2024
Accepted: 06.11.2024

PHYSICOCHEMICAL CHARACTERIZATION AND *IN VITRO* DIGESTIBILITY OF MODIFIED AMARANTH PROTEIN/OCTENYL SUCCINIC ANHYDRIDE-MODIFIED CORN STARCH INSOLUBLE COMPLEXES

Juan J. Figueroa-González[1,2], Consuelo Lobato-Calleros[3], Eduardo J. Vernon-Carter[4], Eleazar Aguirre-Mandujano[3], Diana I. López-Monterrubio[3]✉, Jose Alvarez-Ramirez[4]

[1]Departamento de Ingeniería Agroindustrial, Posgrado en Ciencia y Tecnología Agroalimentaria, Universidad Autónoma Chapingo Km. 38.5, Carretera México-Texcoco, 56230 Texcoco, **México**
[2]Campo Experimental Zacatecas, INIFAP Km. 24.5 Carretera Zacatecas-Fresnillo, 98500 Calera de Víctor Rosales, Zacatecas, **México**
[3]Departamento de Preparatoria Agrícola, Universidad Autónoma Chapingo Km. 38.5, Carretera México-Texcoco, 56230 Texcoco, **México**
[4]Departamento de Ingeniería de Procesos e Hidráulica, Universidad Autónoma Metropolitana-Iztapalapa Ferrocarril San Rafael Atlixco 186, Col. Leyes de Reforma 1ª Sección, CDMX, 09310, **México**

ABSTRACT

Background. Biopolymers can be modified to induce and enhance complexation with other molecules. This study aimed to: (a) obtain insoluble complex coacervates (ICC) via electrostatic interactions between native (N) and modified amaranth protein (AP) using pH shifting (pH 12) and ultrasonication (US), or dual treatment (pH 12-US) with gelatinized octenyl succinic anhydride-modified corn starch (CS_{OSA}); and (b) evaluate the structural, rheological, thermal, morphological and digestibility properties of the ICC variants.
Material and methods. Protein-polysaccharide ICC variants were prepared via electrostatic interactions at pH 3.5 and designated as AP_N-CS_{OSA}, AP_{US}-CS_{OSA}, AP_{pH12}-CS_{OSA} and AP_{pH12US}-CS_{OSA}. These variants were evaluated for ζ-potential, secondary structure and starch band, *in vitro* digestibility, rheology, calorimetry, morphology, sulfhydryl groups and disulfide bonds.
Results. Protein modification significantly influenced the starch band and the proportions of major secondary structure components (β-sheet, random coil, α-helix and β-turn) in the ICC variants. *In vitro* protein digestibility was highest in AP_N-CS_{OSA} (98.1 ±0.52%) and AP_{pH12US}-CS_{OSA} (98.3 ±0.91%). All ICC variants showed a significant increase in the slowly digestible starch fraction. The pasting temperature was highest for AP_N-CS_{OSA} (88 ±0.8°C) and lowest for AP_{pH12}-CS_{OSA} (55 ±1.3°C). Starch retrogradation was lowest for AP_{pH12US}-CS_{OSA} (43 ±0.37%) and highest for AP_N-CS_{OSA} (63 ±1.1%).
Conclusion. Vegetable by-products, such as proteins and starch, can be effectively used to form ICCs. However, they require prior modification through chemical and/or physical methods to optimize their techno-functional properties and digestibility.

Keywords: modified amaranth protein, pH-shifting, ultrasound, OSA-modified corn starch, insoluble complexes

✉ilopezmonterrubio@gmail.com, https://orcid.org/0000-0003-3958-4923

INTRODUCTION

The use of biopolymers with low production costs, such as plant proteins and polysaccharides, is increasingly common to improve the quality and nutritional value of food products (Lin et al., 2017). However, protein modification is essential for enhancing techno-functional properties and expanding commercial applications (Kamani et al., 2022). Native proteins from grains and seeds can be modified through physical (e.g., ultrasound, high-speed shearing), chemical (e.g., pH-shifting), or combined methods to improve or develop new techno-functional properties (Kamani et al., 2022). Many globular proteins undergo conformational changes when exposed to extreme pH conditions, leading to increased repulsions between side chains and partial unfolding of the protein's tertiary structure, often referred to as the molten globule state (Nissen et al., 2021). For instance, pH-shifting has been used to enhance the hydrophobicity of soybean protein isolate for preparing sub-micron gel particles (Yang et al., 2020). The solubility, exposure of hydrophobic residues, and emulsifying activity of Gingko seed proteins were also affected by pH-shifting (Zhang et al., 2021b). On the other hand, ultrasound can alter the physical and even chemical/biochemical properties of proteins by applying high-shear energy waves and cavitation effects in a cost-effective manner. Quinoa protein isolate subjected to ultrasound (5–35 min) showed improved water and oil binding capacities, as well as enhanced emulsifying properties (Mir et al., 2019). Dual pH-shifting (pH 12.5) and sonication (20 kHz) treatment increased the solubility, free sulfhydryl content, and surface hydrophobicity of rapeseed protein isolates (Li et al., 2020). Native amaranth protein subjected to pH-shifting (pH 2 and pH 12) combined with ultrasound (50% amplitude, 10 min) showed increased protein solubility, foaming capacity, and stability, with optimal results under basic pH-shifting (Figueroa-González et al., 2022).

Protein-polysaccharide mixtures can also enhance the stability of dispersed systems. Cationic and anionic biomolecules interact through electrostatic forces to form complex molecular organizations. Insoluble complexes occur when intermolecular electrostatic interactions between biopolymers are sufficiently strong, leading to a net charge close to zero. This results in liquid-liquid phase separation, with one phase being solvent-rich (equilibrium phase) and the other phase enriched in complexes (complex coacervate) (Rodríguez-Rodríguez et al., 2018). The functional properties of these complexes are typically superior to those of individual biopolymers. Heating protein-polysaccharide complexes above the protein denaturation temperature can significantly improve the stability of the particles, making them more suitable as carrier and delivery systems for nutrients (Jones et al., 2009). Wu et al. (2020) investigated the formation of complexes between whey protein isolate (WPI) and octenyl succinic anhydride-modified corn starch (CS_{OSA}), finding that the CS_{OSA} was more likely to interact with heated (90°C, 20 minutes) WPI than non-heated WPI. Heated WPI formed soluble complexes with CS_{OSA} driven by electrostatic interactions, while the structural properties of these complexes were determined by hydrophobic interactions. There is limited information on the digestibility of protein-polysaccharide complexes, as well as their influence on the digestibility of starchy foods, which has led to growing research interest in this area. Feng et al. (2020) studied the effects of ionic polysaccharides – chitosan (C), sodium alginate (A), and xanthan gum (X) – on the *in vitro* starch digestibility of wet sweet potato vermicelli (SPV) when forming binary complexes with egg white protein (EP) (C-EP, A-EP, X-EP). The addition of all the complexes significantly increased the readily digestible starch fraction and reduced the resistant starch fraction in SPV, compared to the control SPV without the addition of complexes.

The aim of this study was to: (a) obtain variations of insoluble complex coacervates through the electrostatic interaction between native or modified amaranth protein variants (modified via pH-shifting at pH 12, ultrasonication, or dual pH shifting/ultrasonication treatment) and gelatinized CS_{OSA}; and (b) evaluate the structural, rheological, thermal, morphological properties, as well as the *in vitro* starch and protein digestibility of the resulting protein-polysaccharide insoluble complex coacervates.

MATERIALS AND METHODS

Materials

Amaranth (*Amaranthus* spp.) seeds of the criollo Amilcingo variety were provided by INIFAP, Zacatepec

ExperimentalField(18º39'20.97"Nand99º12'01.44"W, elevation of 919 m above sea level), in the State of Morelos, Mexico. Native corn starch (CS; CAS number 9005-25-8, moisture content 10.5%, pH 4.8; ash content 0.5%, protein content 0.1%), and the enzymes used for *in vitro* digestibility analysis – pancreatic trypsin (Type IX, 15,310 units/mg protein), bovine pancreatic chymotrypsin (Type II, 48 units/g solid), porcine intestinal peptidase (P-7500, 115 units/mg solid), bacterial protease (Type XIV, 4.4 units/mg solid), amyloglucosidase (A9913), and amylase (A4862) – were purchased from Sigma-Aldrich Mexico (Toluca, State of Mexico, Mexico). Sodium hydroxide, hydrochloric acid, ethanol, and hexane were purchased from J.T. Baker (Xalostoc, State of Mexico, Mexico). Deionized water (DW) was used in all tests.

Extraction of amaranth protein isolate

Amaranth flour (AF) was prepared by grinding amaranth grains in a Nutribullet™ food processor (NB--101B, Hong Kong, Ltd., Guandong, China) and sieving through a No. 80 mesh screen (Manufacturers of Industrial and Commercial Supplies, St. Louis, MO, USA). The AF was degreased using hexane in a Soxhlet apparatus for 5 hours. The defatted AF was then dispersed in deionized water (DW) at a 1:8 w/v ratio, and the protein was solubilized by adjusting the pH to 11.0 with 2.5 N NaOH under constant stirring for 2 hours. The mixture was centrifuged (Eppendorf Centrifuge 5810 R, Hamburg, Germany) at 7168 × g and 20°C for 15 minutes. The supernatant was filtered through Whatman No. 1 filter paper and stored at 4°C for 16 hours. Afterward, the supernatant was shaken (IKA-WERKE Magnetic Stirrer RO15, Staufen, Germany) at 500 rpm for 10 minutes, and the protein was precipitated by adjusting the pH to 4.0 (isoelectric point) with 2.5 N HCl under constant stirring for 2 hours. The suspension was centrifuged as before. The precipitate was washed three times with acidified DW (pH 4, 1:5 w/v ratio) and centrifuged. The protein precipitate was dispersed in DW (1:5 w/v ratio), neutralized to pH 7 with 2.5 N NaOH, and dried at 35°C for 45 hours in an air circulation oven (Riossa Digital HCF-62, Mexico City, Mexico). The resulting native amaranth protein isolate (AP_N) was finely ground using a mortar and stored at room temperature (22 ±2°C) in amber bottles until further use. A specific conversion factor of 5.85 was used to determine the protein content of AP_N (Paredes-López, 2018). Fat, ash, fiber, and protein were analyzed according to AOAC (1996) methods.

Modified amaranth protein variations

AP_N (30 mg/mL) was dispersed in deionized water (DW), stirred for 1 hour at room temperature (22 ±2°C), and then heated to 90°C for 20 minutes. The heated AP_N was used to obtain modified amaranth protein variations by: (a) adjusting the pH of AP_N to 12.0 (pH-Meter H1221, Hanna Instruments, Mexico City, Mexico) with 2.5 N NaOH. The dispersion was kept at room temperature for 1 hour, then the pH was adjusted back to 7.0 with 2.5 N HCl and stirred continuously for 1 more hour. The sample was coded as AP_{pH12}; (b) AP_N was subjected to ultrasonication (US) using an 8 mm diameter stainless steel probe (Ultrasonic Processor, VCX 130 PB 500/750 W, Sonics and Materials, Inc., Newton, CT, USA) for 10 minutes at an amplitude of 50%, using an ice bath. The sample was coded as AP_{US}; (c) A sample of AP_{pH12} was subjected to US as described in (b). The resulting modified protein variation was coded as AP_{pH12US}.

Modification of corn starch by Octenyl Succinic Anhydride (OSA) esterification

The procedure described by Lopez-Silva et al. (2019) was followed. Corn starch (CS, 30 g dry weight) was dispersed in 100 mL of deionized water (DW) with gentle stirring. The pH was adjusted to 8.75 using 0.1 N NaOH, and 3 w/w % OSA (relative to the dry weight of corn starch) was added. The OSA was introduced in six aliquots at 20-minute intervals, with the pH maintained at 8.75 throughout the process. The mixture was allowed to react for 4 hours. Afterward, the pH was adjusted to 7.0 using 0.1 N HCl, and the mixture was centrifuged at 2268 × g at 20°C for 10 minutes (Allegra TM64R centrifuge, Beckman Coulter, Brea, CA, USA). The sample was washed three times with DW and one with 70% ethanol. Finally, the sample was dried at 40°C for 24 hours. The resulting powder was coded as CS_{OSA}. The apparent amylose content was calculated from the ratio of absorbance measurements at 620/510 nm using a Spectronic GENESYS 2 UV–vis Spectrophotometer (Thermo Fisher Scientific, Inc. Waltham, MA, USA).

Preparation of stock solutions

Aqueous dispersions (5% w/v) of the different amaranth protein variations (AP_N, AP_{pH12}, AP_{US}, AP_{pH12US}) were maintained under magnetic stirring (500 rpm) for 2 hours at room temperature and stored overnight at 4°C to ensure full hydration. The pH of the dispersions was adjusted to 7.0 using 0.5 N NaOH and centrifuged at 1000 × g at 20°C for 30 minutes to separate the insoluble protein fractions (Cuevas-Bernardino et al., 2018). An aqueous dispersion (2.5% w/v) of CS_{OSA} was kept under magnetic stirring (500 rpm) for 2 hours at room temperature. The dispersion was then heated in a water bath at 95°C for 20 min to ensure complete gelatinization of the starch. To prevent starch retrogradation, the gelatinized CS_{OSA} dispersion was freshly prepared at the start of each experiment.

ζ-potential

The pH values of the stock solution samples were adjusted to a range between 3 and 6, at 0.5 pH intervals, using 0.1 N NaOH, and then diluted with deionized water (DW) to a concentration of 0.1% w/v. The diluted samples were discharged into a capillary cell of a Zetasizer Nano ZS90 analyzer (Malvern Instruments, Malvern, Worcestershire, UK). The ζ-potential was determined by measuring the direction and velocity of the dispersed molecules as they moved along the applied electric field. The equipment's software converted the electrophoretic mobility measurements into ζ-potential values using the Smoluchowski mathematical model.

Formation of the Insoluble Complex Coacervates (ICC)

The interactions between CS_{OSA} and the different amaranth protein variations (AP_N, AP_{pH12}, AP_{US} and AP_{pH12US}) are driven by attractive electrostatic forces. Based on the ζ-potential-pH behavior of the individual biopolymers, a pH was selected where the maximum absolute value of the product between the negative ζ-potential of the gelatinized CS_{OSA} and the positive ζ-potential of AP_N, AP_{pH12}, AP_{US} and AP_{pH12US} occurred, and where the negatively and positively charge densities were more balanced (Espinosa-Andrews et al., 2008). The selected pH was 3.5 (Fig. 2a). The relative weight ratios at which the negatively charged CS_{OSA} and the positively charged modified amaranth protein variations should be mixed to obtain the ICC were determined as follows: 10 mL (0.02 mg/mL) of the AP variations at pH 3.5 were loaded into the capillary cell of the Zetasizer Nano ZS90 analyzer, and ~0.25 mL aliquots of CS_{OSA} (0.5 mg/mL) at pH 3.5 were titrated into the capillary cell using the MPT-2 equipment autotitrator. Changes in ζ-potential and mean hydrodynamic diameter (d_h) were monitored and recorded by the instrument's software. The optimal mass ratio for ICC formation between the various AP variations and CS_{OSA} was identified as the point where the d_h began to decrease sharply and the ζ-potential approached zero. The selected mass ratios for the different AP variations with gelatinized CS_{OSA} were: 1:0.25 for AP_N-CS_{OSA}, AP_{pH12}-CS_{OSA}, AP_{US}-CS_{OSA}, and 1:1 for AP_{pH12US}-CS_{OSA} (Fig. 2b).

FTIR Spectra

Samples were transferred onto 96-well IR-transparent Siplates and dried in an air circulation Riossa oven at 30°C for 12 hours. Five replicated FTIR samples were prepared to account for possible variations. Infrared spectra were recorded using an FTIR spectrophotometer (Frontier, Perkin Elmer, Mexico City, Mexico), equipped with a universal attenuated total reflectance (ATR) accessory. Dried ground samples (~10 mg) of the AP variations, gelatinized CS_{OSA}, and the different ICC were placed in contact with the diamond crystal, with geometry adjusted using a force gauge (60 units). Absorbance was measured over the wavelength range of 4000–400 cm^{-1} with a resolution of 40 cm^{-1}. Quantitative analysis of the FTIR spectra was performed using numerical least-squares deconvolution with Gaussian basis functions with the OriginLab® (Version 2018) software package. The baseline was removed for all cases. Specifically, the Amide I region (1700–1600 cm^{-1}) was analyzed to assess the protein secondary structure and identify the relevant peaks. Numerical least-squares deconvolution was also applied to the starch band in the range of 1200 and 900 cm^{-1} to determine the ordered structures of the external starch region. Gaussian peaks were assigned to the corresponding structures based on their center, and the integral of each peak was divided by the sum of all determined peaks. This allowed for the calculation of the proportion (%) of each structure in both the amaranth protein and starch.

In vitro digestibility

In vitro protein digestibility (IVPD)

The different AP and ICC variations (63.8 mg each) were separately dissolved in 10 mL of deionized water (DW). The pH was adjusted to 8.0 using 1 N NaOH, and the samples were agitated continuously in a water bath until they reached 37°C. To each sample, 1 mL of enzyme solution (1.58 mg of trypsin, 3.65 mg of chymotrypsin and 0.45 mg of peptidase) was added while stirring in the water bath (37°C). Immediately, 1 mL of bacterial protease (1.48 mg) was added, and the samples were stirred at 55°C for 10 minutes. After cooling to room temperature (22 ±2°C), the pH was measured to estimate IVPD according to the methods of Hsu et al. (1977) and Rothenbuhler and Kinsella (1985). Briefly, the initial pH was recorded before enzyme addition and then recorded at 30-second intervals over a 10-minute period. The pH drop in *in vitro* protein digestibility (IVPD, %) was calculated using the following formula:

$$IVDP(\%)_{pH\text{-}drop} = 65.66 + 18.10 \times \Delta pH_{min}$$

In vitro starch digestibility

The *in vitro* digestion of the gelatinized CS_{OSA} and the ICC variants was performed following the methodology proposed by Lee et al. (2019) with slight modifications. In brief, pancreatic α-amylase (0.0225 g, 10 U/mg) was suspended in 7.5 mL sodium acetate buffer (0.02 M, pH 5.5) with stirred magnetically for 30 minutes, followed by centrifugation at 1500 × g for 5 min. The supernatant was transferred into a beaker and mixed with 0.75 mL of amyloglucosidase (300 U/mL). This enzyme solution was prepared freshly and equilibrated at 37°C for 10 minutes before each test. ICC and starch samples (0.5 g) were dispersed in 25 mL of deionized water (DW) and equilibrated at 37°C for 10 minutes in a water bath. The enzyme solution (0.75 mL) was then added to samples, which were incubated at 37°C with gentle shaking for 120 minutes. Aliquots were taken at 0, 20 and 120 minutes. For quantitative determination of reducing sugars, the DNS method was used (Miller, 1959). A standard curve was prepared by measuring the absorbance at 540 nm of known concentrations of glucose solutions. Measurements were made in duplicate for each sample, and the data presented are the averages of these results.

The percentages of readily digestible starch (RDS), slowly digestible starch (SDS), and resistant starch (RS) in the samples were calculated using the following equations:

$$RDS(\%) = \frac{G20 - FG}{TS} \times 0.9 \times 100$$

$$SDS(\%) = \frac{G120 - G20}{TS} \times 0.9 \times 100$$

$$RS(\%) = ((TS - RDS + SDS)/TS) \times 100$$

where:

RDS is the rapidly digestible starch
SDS is the slowly digestible starch
RS is the resistant starch
G20 and *G120* are the amounts of glucose released after 20 and 120 minutes, respectively
FG is the amount of free glucose in the original sample
TS is the total starch weight of the original sample (Ye et al., 2019).

Pasting properties

The pasting profiles of aqueous dispersions of ICC variants (1.5 mL, 5% w/w, pH 3.5) were determined as described by Mendez-Montealvo et al. (2011), with slight modifications. A rotational test was performed using a Physica MCR 301 rheometer (Anton Paar, Messtechnik, Stuttgart, Germany) with a plate-plate geometry (25 mm diameter; 1 mm gap), at a heating or cooling rate of 2°C/min and a constant shear rate of 50 s^{-1}. To prevent water evaporation during the test, the edge of the geometry was covered with glycerin. The rheometer was programmed to run heating sweeps from 25°C to 90°C, hold at 90°C for 10 minutes, cool the sample from 90°C to 25°C, and hold at 25°C for 5 minutes.

Figure 1 shows a schematic representation of typical pasting profiles and the parameters that can be obtained from them (Park et al., 2007). The parameters measured were: pasting onset temperature (PO), peak temperature (PT), peak viscosity (PV), trough viscosity (TV), final viscosity (FV), breakdown viscosity (BV), and setback viscosity (SB).

- **PO** is the temperature at which the viscosity of a substance begins to increase
- **PV** is the maximum viscosity reached during the heating and holding cycle

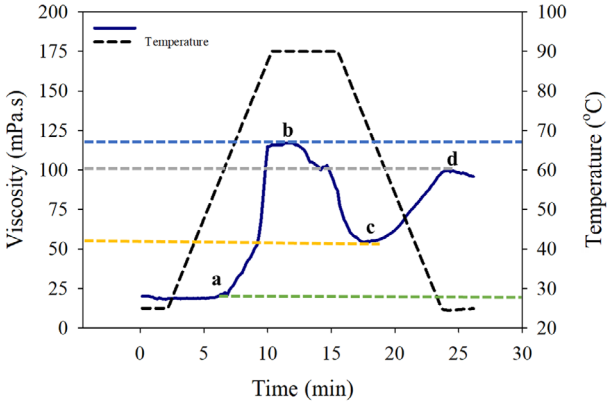

------- indicates temperature profiles; a: pasting onset temperature (PO); b: peak viscosity (PV) and peak temperature (PT); c: trough viscosity (TV); d: final viscosity (FV).

Fig. 1. Pasting profiles obtained with a rotational rheometer

- **PT** is the temperature at which the substance reaches its peak viscosity (PV)
- **TV** is the minimum viscosity reached after the PV
- **FV** is the viscosity at the end of the test.

These parameters are used to describe the pasting properties of substances like starch. Additional parameters related to pasting properties include:

- **Breakdown viscosity (BV)**, the difference between the PV and TV
- **Setback viscosity (SV)**, the difference between the PV and FV.

Differential Scanning Calorimetry (DSC)

The thermal properties of the different ICC variants were measured using a DSC (Q1000, TA Instruments, New Castle, DE, USA). Dried ICC (5 mg, dry basis.) was weighed and placed in an aluminum pan (40 µL, diameter 5 mm), to which 10 µL of deionized water (DW) (pH 3.5) was added. The samples were then hermetically sealed and allowed to equilibrate for 24 hours at 4°C before being heated in the DSC. The sample was subjected to a heating ramp from 20°C to 200°C in a heating rate of 10°C/min.

The thermal properties associated with the gelatinization of the ICC were determined by measuring changes in enthalpy (ΔH in J g^{-1} of dry ICC), as well as the initial temperature (T_o), peak temperature (T_p), and conclusion temperature (T_c). After thermal analysis, the samples were stored at 4°C for 7 days to investigate ICC retrogradation. Retrogradation enthalpy (ΔH_{ret}) was automatically calculated, and the retrogradation percentage (% R) was determined using the following formula:

$$\%R = 100 \times \Delta H_{ret} / \Delta H_{gel}.$$

Scanning Electron Microscopy (SEM)

The samples were dried according to the procedure described for FTIR analysis. A small amount (approximately 0.1 g) was placed onto a piece of aluminum using double-sided tape. Protein particles were mounted on carbon sample holders using double-sided sticky tape and were observed using a JEOL JMS 7600F scanning electron microscope (Akishima, Japan), operating in GB-H mode at an accelerating voltage of 1 kV. Micrographs were captured at a magnification of 3000×.

Sulfhydryl groups (SH) and disulfide bonds (SS)

A 4 mg solution of DTNB (Ellman's Reagent; 5,5-dithio-bis-2-nitrobenzoic acid) was freshly prepared by dissolving it in 1 mL of buffer (0.05 M sodium phosphate and 0.1 M sodium chloride, pH 7). To determine free sulfhydryl groups (SH_f), 15 mg of ICC were dissolved in 10 mL of buffer, and 50 µL of DTNB solution was added. The mixture was stirred for 1 hour at room temperature and then centrifuged at 7168 × g for 15 minutes at 15°C. The absorbance of the supernatant was measured at 412 nm (Thermo Fisher Scientific, Waltham, MA, USA).

To identify exposed sulfhydryl groups (SH_e), the same procedure as for SH_f was followed, but without buffer, and the protein was dissolved in 10 mL of 8 M urea. The total sulfhydryl content (SH_t) was determined by dissolving the ICC in 10 mL of 8M urea, then adding 50 µL of mercaptoethanol and 50 µL of DTNB. The disulfide bonds content (SS) was calculated as the difference between SH_t–SH_e. The sulfhydryl SH content was calculated using the extinction coefficient of DTNB (13600 M^{-1} cm^{-1}) and expressed as µmol/g of protein.

Statistical analysis

All measurements were conducted in triplicate across three independent experiments. The results are expressed as mean values ±standard deviation. Data

were analyzed using ANOVA, and where appropriate, Tukey's test was used for mean comparisons. Statistical significance was defined as $p \leq 0.05$ (SAS version 9.4, SAS Institute Inc., NC, USA).

RESULTS AND DISCUSSION

Composition

The composition of the defatted AF (% w/w, dry weight basis) was as follows. Ash: 3.45 ±0.46, protein: 18.08 ±0.65, fat: 0.42 ±0.05, fiber: 3.31 ±0.08, and carbohydrates: 73.50 ±0.63. The AP_N yield was 5.02 ±0.48% w/w, with a protein content of 83.29 ±1.02% w/w (dry weight basis, db).

ζ-potential of biopolymers and ICC

The ζ-potential values of the AP variations and gelatinized CS_{OSA} are presented in Figure 2a. The ζ-potential of the different AP variation dispersions ranged from 26.4 ±1.75 (pH 3.0) to –28.6 ±1.06 mV (pH 6.0). Negative ζ-potential values were observed when the pH of the medium exceeded the isoelectric point (pI) of the AP variations. The pI of the AP variations fluctuated between about 3.6 for AP_{US} to 4.0 for AP_{pH12US} (Fig. 2a). This behavior can be attributed to the ionization of carboxylic groups (COOH) to carboxylate groups (COO^-), while positive ζ-potential values at pH values below the isoelectric point result from the protonation of amino residues (NH_2) which form ammonium groups (NH_3^+) (García-de la Rosa et al., 2023).

The negative ζ-potential values exhibited by the AP variations increased from pH 4.5 to pH 6.0, with the following trend from more negative to less negative: $AP_N > AP_{US} > AP_{pH12} > AP_{pH12US}$ (Fig. 2a). Fluctuations in the ζ-potential values are affected by the pI of the different AP variations, which defines the pH at which the carboxylic acid ionization commences, as well as the method used to alter the protein structure. Different methods impact the protein structure in different ways, potentially exposing new functional groups while burying previously exposed ones (Nazari et al., 2018). For example, US treatment can induce partial unfolding of the native protein, exposing new functional groups that were previously buried within the interior (Zhang et al., 2021a). If these newly exposed groups carry positive charges, they may neutralize the negative charges of the functional groups that were present on the surface before treatment (Yang et al., 2023).

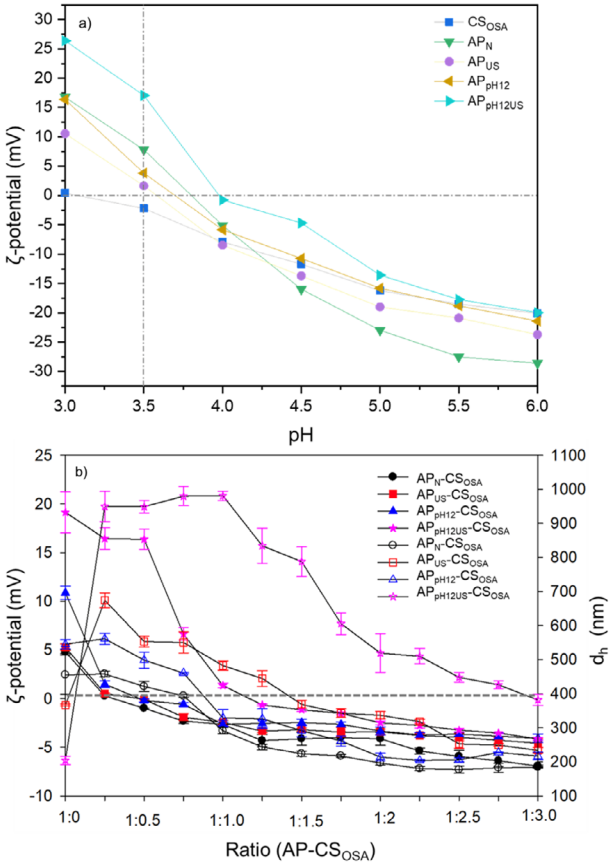

Respectively a) ζ-potential of insoluble complex coacervates (ICC) of native (AP_N) and modified (AP_{US}, AP_{pH12} and AP_{pH12US}) amaranth protein with CS_{OSA}, b) filled symbols represent the ζ-potential, and empty symbols represent the d_h.
The vertical bars represent the SD.

Fig. 2. ζ-potential of the gelatinized octenyl succinic anhydride-modified corn starch (CS_{OSA}), native (AP_N), and modified (AP_{US}, AP_{pH12} and AP_{pH12US}) amaranth proteins using ultrasonication, pH shifting and dual modification

The ζ-potential values for gelatinized CS_{OSA} ranged from 0.01 ±0.001 (pH 3.0) to –20.6 ±0.20 mV (pH 6.0). The consistently negative values across the entire pH range are due to the low pK_a values of the carboxyl groups. The maximum stoichiometric difference between the positively charged AP variations and the negatively charged gelatinized CS_{OSA} occurred at a pH value of 3.5 (pH_{esteq}), which was used for the formation of all ICCs.

The ζ-potential values for the different ICC variations ranged between 19.3 ±2.10 to –4.5 ±0.44 mV. The mass ratio used to form the AP_N-CS_{OSA}, AP_{US}-CS_{OSA} and AP_{pH12}-CS_{OSA} insoluble complexes was 1:0.25, while for AP_{pH12US}-CS_{OSA}, it was 1:1. At these mass ratios, the ζ-potential presented values were close to zero, indicating that the protein molecules had enough binding sites to immediately saturate the negative charge of the polysaccharide at pH at 3.5, independently of the AP treatment used in the formation of ICCs (Fig. 2a). When the gelatinized CS_{OSA} molecules were in excess, all the positive charges of the protein molecules were neutralized and, thus, the gelatinized CS_{OSA} molecules dominated the overall charge of the system. Additionally, the ICC variations exhibited maximum d_h values at pH 3.5 (Fig. 2b). The maximum particle size of the ICCs ranged from 458.7 ±7.9 nm for AP_N-CS_{OSA} to 631.5 ±24.1 nm for AP_{US}-CS_{OSA}, 461.2 ±16.2 for AP_{pH12}-CS_{OSA} and 949.4 ±44.3 nm for AP_{pH12US}-CS_{OSA}. Xu et al. (2021) reported a particle size value of 832.3 ±33.2 nm for OSA-modified corn starch/chitosan complex.

FTIR analysis

Proteins

The FTIR spectra of the different AP variations are shown in Figure 3a. The peaks between 3283 and 3262 cm^{-1} correspond to the amide A band, attributed to the stretching vibrations of the N–H and O–H bonds, which are intermolecularly bonded through hydrogen bridges. In the case of AP_N, these peaks shifted to lower wavenumbers compared to AP_{US}, AP_{pH12} and AP_{pH12US}, likely due to the hydrogen bonds between protein molecules. The amide I band, which ranges from 1700 to 1600 cm^{-1}, arises primarily from C=O stretching vibrations, C–N stretching and N–H bending vibrations. FT-IR is commonly used to detect modifications in the secondary structure of proteins resulting from various treatments (Flores-Silva et al., 2022). Changes in the amide I band peak reflect alterations in the protein's secondary structure.

The secondary structure components vary, with the β-sheet typically presenting bands between 1638–1610 cm^{-1}, the random coil between 1648–1638 cm^{-1}, the α-helix between 1660–1649 cm^{-1} and the β-turn observed at 1652 cm^{-1} or between 1691–1672 cm^{-1}. The four main structural components making up the secondary structure of the AP variations were β-sheet, random coil, α-helix, and β-turn (Table 1, Fig. 3). Among these, β-sheet was the predominant component in AP_N (Fig. 3b) and AP_{pH12US} (Fig. 3e) followed by random coil, while random coil was the primary component in AP_{US} (Fig. 3c) and AP_{pH12} (Fig. 3d).

The β-sheet is the most tightly packed structure in a protein molecule. It was expected that AP_N, subjected only to thermal treatment, would exhibit a high proportion of this component. In contrast, for AP_{pH12US}, it was expected that the combination of pH shifting + US treatment would disrupt the secondary structure. However, the observed increase in β-sheet content suggests that the highly unfolded protein molecules induced by the combined treatment likely formed aggregates (Yang et al., 2022). In AP_{US} and AP_{pH12}, the protein molecules were less unfolded compared to the combined US-pH shifting treatment, resulting in an increase in random coil and α-helix components at the expense of the β-sheet component. These alterations in secondary structure contributed to changes in the overall protein structure. Additionally, a higher α-helix content enhanced the stability and flexibility of the protein.

Insoluble Complex Coacervates

The structural components of the protein and starch bands of the different ICC variations are shown in Figure 4, with numerical values provided in Table 1. The β-sheet content increased from 8.5 ±0.6% in AP_N-CS_{OSA} (Fig. 4a) to 20.5 ±1.4 in AP_{pH12}-CS_{OSA} (Fig. 4e) and 25.8 ±1.7% in AP_{pH12US}-CS_{OSA} (Fig. 4g), decreasing to 1.5 ±0.4% in AP_{US}-CS_{OSA} (Fig. 4c). These results contrast with the β-sheet contents, which were significantly higher in the individual AP variations compared to the ICC variations. Similarly, the random coil component was greater in the AP variations than in the ICC variations, except for AP_{pH12US}. Conversely, all ICC variations exhibited significantly higher α-helix content compared to their corresponding AP variations.

An increase in disordered structures within a protein generally indicates greater conformational changes. The lowest α-helix content observed in AP_{pH12US}-CS_{OSA} can be attributed to the dual pH/ultrasonication treatment, which likely destroyed the hydrogen bonds between the carbonyl group and the amino group in the polypeptide chain, destabilizing the α-helix structure and reducing the α-helix content.

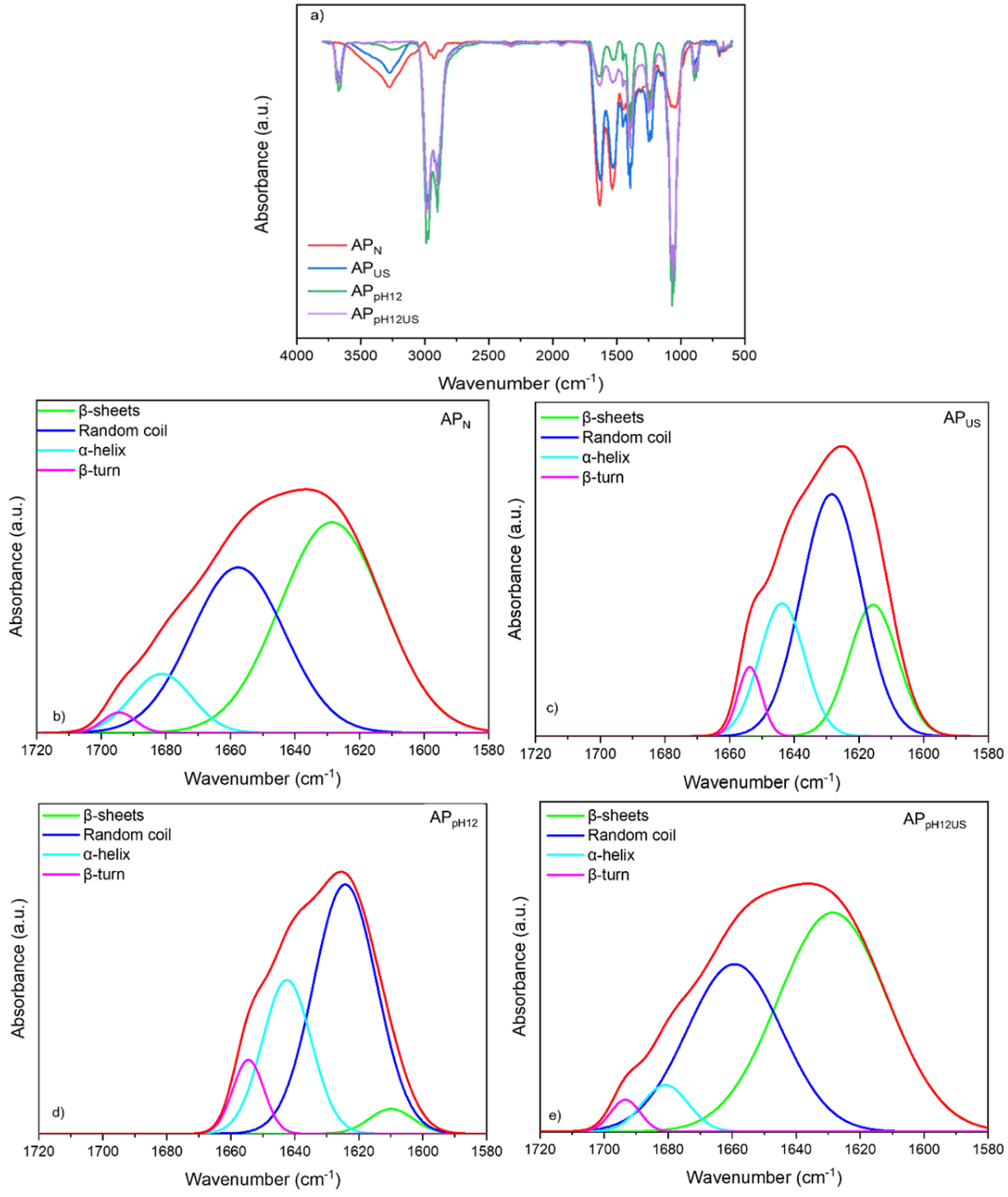

a) gaussian deconvolution of FTIR signals in the Amide I region for native (AP_N) and modified (AP_{US}, AP_{pH12}, and AP_{pH12US}) amaranth proteins using ultrasonication, pH shifting and dual modification, respectively.

Fig. 3. FTIR illustration of the different amaranth protein variations

Table 1. Components of the secondary structure of the different AP and ICC variations

Treatment, %	Component			
	β-sheets	Random coil	α-helix	β-turn
AP_N	53.6 ±2.5[c]	37.3 ±2.5[a]	8.5 ±0.3[a]	1.7 ±0.3[a]
AP_{US}	22.3 ±1.1[a]	51.0 ±2.2[b]	21.0 ±1.7[b]	5.7 ±0.8[b]
AP_{pH12}	41.0 ±0.6[b]	59.1 ±1.1[c]	28.2 ±1.1[b]	8.6 ±0.9[b]
AP_{pH12US}	55.7 ±3.1[c]	37.1 ±2.4[a]	5.0 ±0.1[a]	2.2 ±0.4[a]
AP_N-CS_{OSA}	8.5 ±0.6[b]	33.5 ±0.8[b]	49.8 ±3.1[b]	8.2 ±0.4[b]
AP_{US}-CS_{OSA}	1.5 ±0.3[a]	35.0 ±2.1[b]	55.0 ±1.4[c]	7.7 ±0.3[b]
AP_{pH12}-CS_{OSA}	20.5 ±0.7[c]	25.9 ±2.3[a]	52.8 ±1.3[c]	0.8 ±0.03[a]
AP_{pH12US}-CS_{OSA}	25.8 ±1.7[d]	46.6 ±2.1[c]	18.4 ±0.8[a]	9.2 ±0.7[b]

Values are presented as mean ±SD of triplicates. Different letters in the same rows indicate significant differences ($p \leq 0.05$) between means. AP_N: native amaranth protein; AP_{US}: ultrasonication modified amaranth protein; AP_{pH12}: pH shifting modified amaranth protein; AP_{pH12US}: dual-modified amaranth protein (pH shifting and ultrasonication). Insoluble complex coacervates (ICC) between the different AP variations and gelatinized octenyl succinic anhydride-modified corn starch (CS_{OSA}).

Table 2. FTIR 1047/1022 and 995/1022 ratios for gelatinized octenyl succinic anhydride-modified corn starch (CS_{OSA}) and the different ICC variations

Treatment	1047/1022	995/1022
CS_{OSA}	0.11 ±0.002[a]	0.35 ±0.001[ab]
AP_N-CS_{OSA}	0.81 ±0.015[d]	1.85 ±0.019[d]
AP_{US}-CS_{OSA}	0.46 ±0.001[c]	0.76 ±0.002[c]
AP_{pH12}-CS_{OSA}	0.34 ±0.002[b]	0.38 ±0.001[b]
AP_{pH12US}-CS_{OSA}	0.35 ±0.001[b]	0.38 ±0.001[b]

Values are presented as mean ±SD of triplicates. Different letters in the same column indicate significant differences ($p \leq 0.05$) between means. AP_N: native amaranth protein; AP_{US}: ultrasonication modified amaranth protein; AP_{pH12}: pH shifting modified amaranth protein; AP_{pH12US}: dual-modified amaranth protein (pH shifting and ultrasonication). Insoluble complex coacervates (ICC) between the different AP variations and gelatinized octenyl succinic anhydride-modified corn starch (CS_{OSA}).

The β-turn content did not differ significantly ($p > 0.05$) between AP_N-CS_{OSA} (8.2 ±0.4%), AP_{US}-CS_{OSA} (7.7 ±0.3%) and AP_{pH12US}-CS_{OSA} (9.2 ±0.7%), but was significantly lower ($p \leq 0.05$) in AP_{pH12}-CS_{OSA} (0.8 ±0.01%). Additionally, the 1047/1022 and 995/1022 ratios for the ICC variations (Tab. 2) were significantly higher ($p \leq 0.05$) compared to CS_{OSA}. The increase in the 1047/1022 ratio was consistent with findings reported by Wang et al. (2023) for bean protein-wheat starch complexes, where the presence of protein promoted the formation of an ordered structure within the starch. This facilitated the formation of hydrogen bonds between the protein and the starch hydroxyl groups, leading to the rearrangement of starch chains. This ordered stable starch structure enhances resistance to enzymatic interaction, thereby delaying starch digestion. The increase in the 995/1022 ratio suggests that protein-starch interactions weakened hydrogen bonds between starch molecules, reducing the double helix structure of the starch. Furthermore, the increase in the 995/1022 ratio may be closely associated with the formation of complexes between protein and starch. The 995/1022 ratio was higher for AP_N-CS_{OSA} compared to the other ICC variations. A decrease in this ratio suggests a reduction in the short-range order of the starch, which can be attributed to the starch-protein interactions that restrict the reassembly of the starch chain into ordered helices.

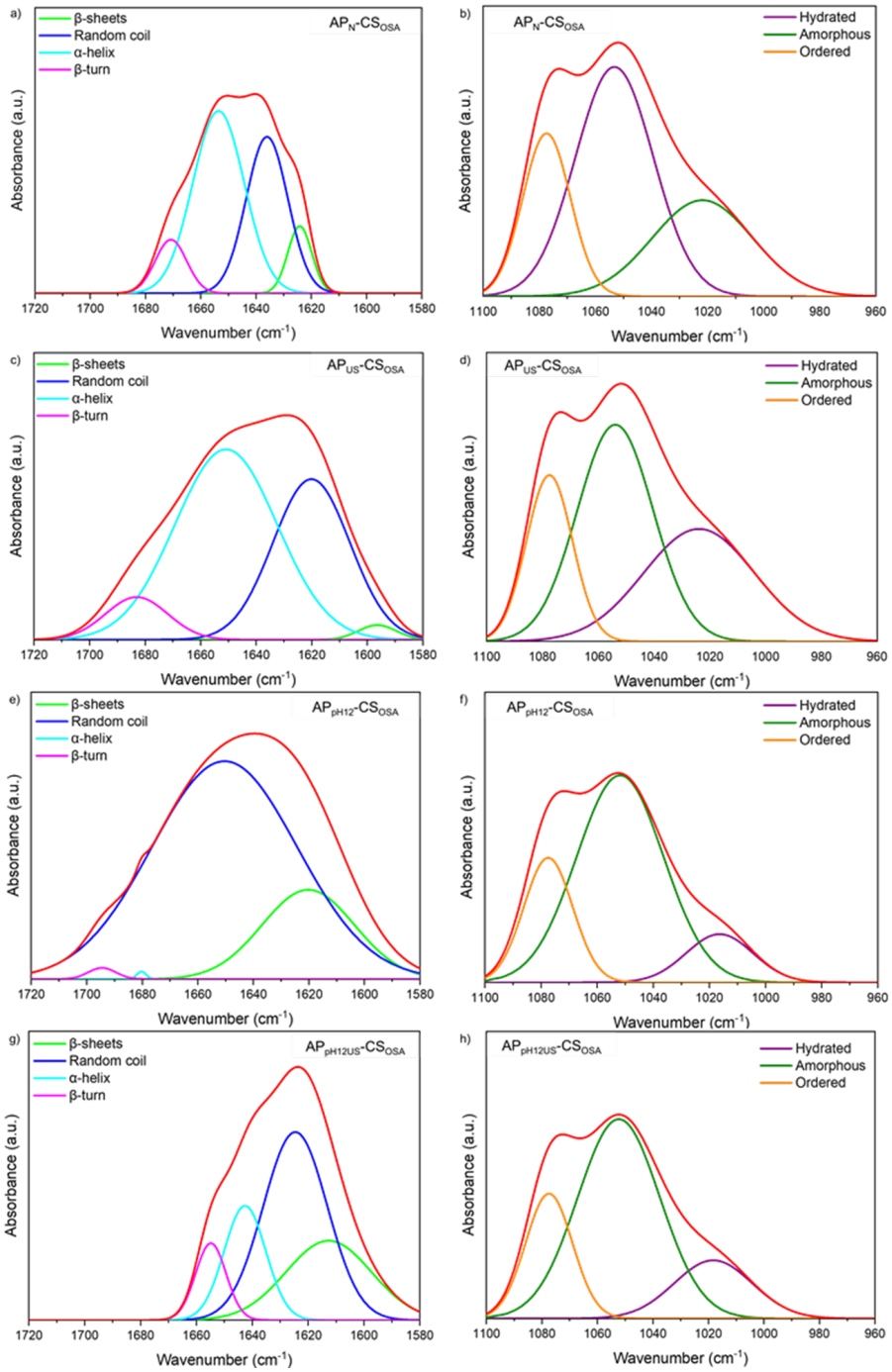

Fig. 4. Gaussian deconvolution of FTIR signals in the Amide I region (a, c, e, g) and illustration of least squares numerical deconvolution in the starch band region (b, d, f, h) of AP_N-CS_{OSA}, AP_{US}-CS_{OSA}, AP_{pH12}-CS_{OSA}, and AP_{pH12US}-CS_{OSA} insoluble complex coacervates of native (AP_N) and modified (AP_{US}, AP_{pH12} and AP_{pH12US}) amaranth proteins using ultrasonication, pH shifting and dual modification, respectively, with gelatinized octenyl succinic anhydride-modified corn starch (CS_{OSA})

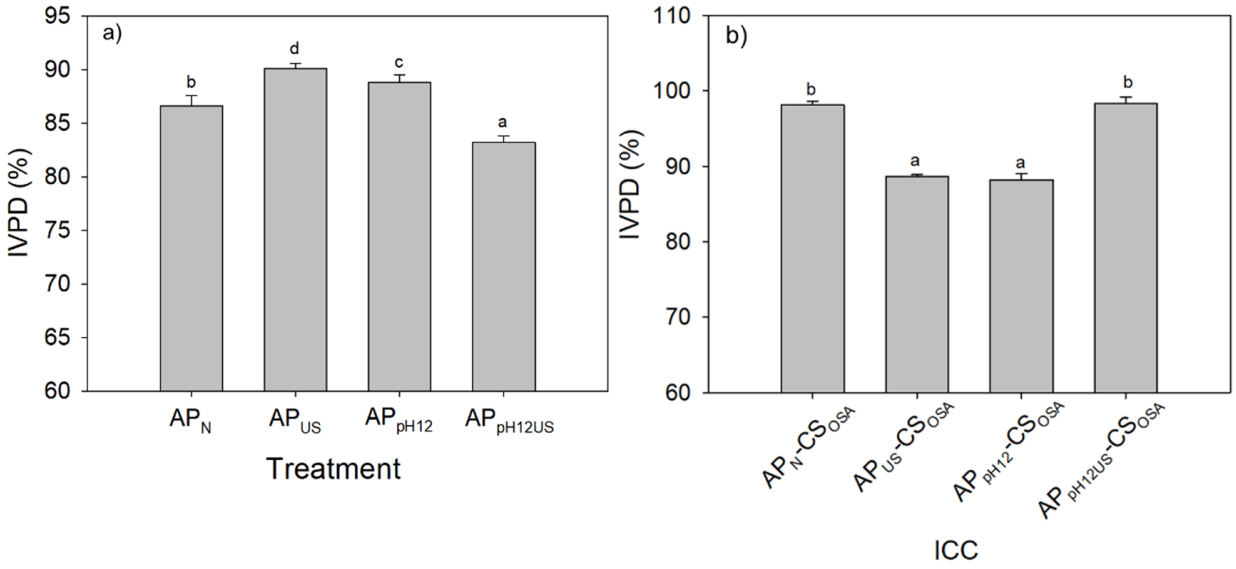

Respectively, a) insoluble complex coacervates of native (AP_N) and modified (AP_{US}, AP_{pH12} and AP_{pH12US}) amaranth proteins with gelatinized octenyl succinic anhydride-modified corn starch (CS_{OSA}), b) the vertical bars represent the SD.
Different letters indicate significant differences ($p \leq 0.05$) between means.

Fig. 5. Relative *in vitro* protein digestibility of native (AP_N) and modified (AP_{US}, AP_{pH12} and AP_{pH12US}) amaranth proteins using ultrasonication, pH shifting and dual modification

Digestibility

In vitro protein digestibility (IVPD)

Figure 5a shows the IVPD for the different AP variants. The digestibility of AP_N (86.6 ±1.0%) decreased compared to AP_{pH12US} (83.2 ±0.61%) but increased relative to AP_{pH12} (88.8 ±0.73%) and AP_{US} (90.1 ±0.55%). Adequate US conditions altered the protein's conformation, potentially exposing cleavage sites for digestive enzymes. Furthermore, sonication can enhance protein digestibility by inducing changes in secondary structure content through the physical forces of cavitation and free radicals.

High *in vitro* digestibility values have been associated with a high content of random coil structures due to the increased availability of amino acids in disordered structures, which facilitates enzymatic recognition (Carbonaro et al., 2012). In this context, the AP_{US} and AP_{pH12} variants showed the highest random coil content (see Table 1). Conversely, a predominant β-sheet structure has been linked to resistance against denaturation during gastrointestinal digestion (Carbonaro et al., 2015). This could explain the lower digestibility of the AP_{pH12US} variant, which exhibited a predominance of β-sheet structures (see Tab. 1).

Non-significant differences in IVPD (Fig. 5b) were observed between AP_N-CS_{OSA} (98.1 ±0.52%) and AP_{pH12US}-CS_{OSA} (98.3 ±0.91%). However, AP_{US}--CS_{OSA} (88.6 ±0.36%) and AP_{pH12}-CS_{OSA} (88.2 ±0.87%) exhibited significantly lower IVPD values than their respective counterparts. The increased IVPD can be attributed to exposed hydrophobic groups, which enable proteolytic enzymes to create additional binding sites, thereby hydrolyzing the protein structure and eventually increasing IVPD. Bai et al. (2016) reported that the percentage of α-helix structures was positively correlated with the *in vitro* digestibility of vegetable and animal proteins ($R = 0.916$, $p < 0.001$).

In vitro starch Digestibility

The results of the analysis of *in vitro* starch are presented in Table 3. The percentage of the RDS fraction in gelatinized CS_{OSA} was approximately 9.12%. The values for the different ICC variations were lower (by one to two orders of magnitude) than the SDS and RS percentages. Lopez-Silva et al. (2019) reported that

Table 3. Percentage of the readily (RDS), slowly (SDS) and resistant (RS) starch fractions in the gelatinized octenyl succinic anhydride-modified corn starch (CS_{OSA}) and the different ICC variations

Treatment	RDS	SDS	RS
CS_{OSA}	9.12 ±0.89^{d}	90.85 ±1.25^{d}	0.03 ±0.01^{a}
AP_{N}-CS_{OSA}	0.21 ±0.17^{a}	62.80 ±1.64^{d}	36.90 ±1.67^{b}
AP_{US}-CS_{OSA}	0.41 ±0.12^{ab}	46.30 ±0.14^{c}	53.30 ±0.21^{c}
AP_{pH12}-CS_{OSA}	1.23 ±0.40^{b}	47.90 ±0.62^{c}	51.00 ±0.22^{c}
AP_{pH12US}-CS_{OSA}	4.52 ±0.27^{d}	42.10 ±0.37^{b}	53.40 ±0.21^{c}

Values are presented as mean ± SD of triplicates. Different letters in the same column indicate significant differences ($p \leq 0.05$) between means. AP_{N}: native amaranth protein; AP_{US}: ultrasonication modified amaranth protein; AP_{pH12}: pH shifting modified amaranth protein; AP_{pH12US}: dual modified amaranth protein (pH shifting and ultrasonication). Insoluble complex coacervates (ICC) between the different AP variations and gelatinized octenyl succinic anhydride-modified corn starch (CS_{OSA}).

OSA-treated corn starch with varying amylose contents exhibited reduced RDS content compared to untreated corn starches. They suggested that OSA acted as a cross-linking agent between starch chains, thereby reducing amylolysis.

More recently, Li et al. (2024) found that OSA--modified starch-protein complexes exhibited altered structural and functional properties compared to those exhibited by the individual biopolymers. These complexes showed increased RS +SDS contents. Mejía-Terán and Blanco-Tizarazo (2021), in their systematic review of starch-based foods from protein interactions, found that incorporating protein into food matrices reduced starch hydrolysis and digestibility rates. This effect can be attributed to the presence of proteins, which form a physical barrier by adsorbing onto or embedding within the surface of CS_{OSA}, thereby preventing enzymatic recognition of starch by digestive enzymes. The overall effect is a decrease in RDS and an increase in SDS.

The presence of OSA groups also allows amylopectin molecules to cross-link during heat treatment and interact with each other through hydrophobic interactions during enzymatic digestion in an aqueous environment. These cross-linking and hydrophobic interactions can lead to the aggregation of CS_{OSA} molecules and increase their insolubility, reducing enzyme accessibility to CS_{OSA} and making it more slowly digestible.

Pasting properties

The PO in AP_{pH12}-CS_{OSA} was statistically different ($p \leq 0.05$) from the other ICC (Table 4). Low and high PV values were observed in AP_{pH12}-CS_{OSA} and AP_{pH12US}-CS_{OSA}, respectively, suggesting that the dual pretreatment of pH shift/ultrasound and the ratio of AP_{pH12U}S-CS_{OSA} (1:1) enhanced the swelling capacity of the starch granules. The PT in AP_{N}-CS_{OSA} and AP_{pH12}-CS_{OSA} were statistically equal ($p \leq 0.05$) but differed from those in AP_{US}-CS_{OSA} and AP_{pH12US}-CS_{OSA}. The TV in AP_{pH12US}-CS_{OSA} was the highest, followed by AP_{N}-CS_{OSA} and AP_{US}-CS_{OSA}, while the lowest value

Table 4. Pasting properties of the different ICC variations

Treatment	PO °C	PV mPa·s	PT °C	TV mPa·s	FV mPa·s	BV	SV
AP_{N}-CS_{OSA}	29 ±0.1^{b}	75 ±0.3^{c}	34 ±0.3^{a}	65 ±0.8^{c}	73 ±0.4^{b}	10 ±0.1^{b}	2 ±0.2^{a}
AP_{US}-CS_{OSA}	27 ±0.2^{b}	58 ±0.4^{b}	45 ±0.2^{b}	51 ±1.1^{b}	223 ±6.7^{d}	7 ±0.4^{a}	165 ±1.9^{c}
AP_{pH12}-CS_{OSA}	25 ±0.7^{a}	45 ±0.7^{a}	38 ±0.7^{a}	30 ±0.4^{a}	49 ±0.5^{a}	15 ±0.2^{c}	4 ±0.8^{a}
AP_{pH12US}-CS_{OSA}	28 ±0.4^{b}	120 ±2.4^{d}	52 ±0.9^{c}	102 ±1.4^{d}	99 ±1.1^{c}	18 ±0.1^{d}	21 ±0.4^{b}

Values are presented as mean ±SD of triplicates. Different letters in the same column indicate significant differences ($p \leq 0.05$) between means. AP_{N}-CS_{OSA}, AP_{US}-CS_{OSA}, AP_{pH12}-CS_{OSA}, and AP_{pH12US}-CS_{OSA} insoluble complex coacervates of native (AP_{N}) and modified (AP_{US}, AP_{pH12} and AP_{pH12US}) amaranth protein using ultrasonication, pH shifting and dual modification, respectively, with octenyl succinic anhydride-modified corn starch (CS_{OSA}).

was observed in AP_{pH12}-CS_{OSA}. This reduction in TV can be attributed to higher stability during successive heating and shearing, which mitigates the destabilizing effect on the amorphous region of melted crystallites in starch, reducing the ICC's capacity to resist heating and shear stress during heating.

Low TV has been reported in rice starch treated with low-power ultrasound, primarily caused by the degradation and depolymerization of leached amylose and long-chain amylopectin (Yang et al., 2019). Furthermore, low TV values indicate a low tendency for retrogradation and suggest good quality for the consumption of ICC. Likewise, this can be advantageous in formulations where starch stability at low temperatures is required, such as soups, sauces, and puddings, which may experience a loss of viscosity, precipitation and syneresis.

For FV, the lowest value was observed in AP_{pH12}--CS_{OSA}, and the value increased notably in the other ICCs. The increasing viscosities suggest that interactions occurred between starch molecules and amaranth protein, and tend to retrograde after cooling and recrystallization of amylose molecules. The AP_N-CS_{OSA}, AP_{US}-CS_{OSA} and AP_{pH12}-CS_{OSA} complexes exhibited low PT and PV values. This behavior may indicate an incomplete fusion of the amylose double helices, resulting in greater integrity of the partially swollen starch granules.

Thermal properties

The evaluated thermal properties are presented in Table 5. The T_o value decreased with both the single pH-shift and US treatments, and further decreased with the combined treatment, with significant differences ($p \leq 0.05$). Both the T_p and the T_c of the gelatinization process in the different ICCs did not show significant differences ($p \leq 0.05$), which can be attributed to the greater thermal stability of the protein, due to the presence of disulfide bonds within the protein molecule. AP_N-CS_{OSA} exhibited a narrower ΔT range compared to the other ICCs. The widest ΔT range was exhibited by AP_{US}-CS_{OSA}, AP_{pH12}--CS_{OSA} and AP_{pH12US}-CS_{OSA}, which may reflect the number of double helices and the heterogeneity of starch crystals during the gelatinization process. AP_N-CS_{OSA} presented lower ΔH_{gel} values compared to AP_{pH12}-CS_{OSA}, AP_{US}-CS_{OSA} and AP_{pH12US}-CS_{OSA}. Significant differences were observed between all samples ($p \geq 0.05$). An

Table 5. Thermal properties (gelatinization and retrogradation) of the different ICC variations

Treatment	Retrogradation				
	T_o, °C	T_p, °C	T_c, °C	ΔT, °C	ΔH_{gel}, j/g^{-1}
AP_N-CS_{OSA}	160 ±1.2^c	167 ±0.3^a	169 ±0.1^a	9.7 ±1.1^a	81 ±0.2^a
AP_{US}-CS_{OSA}	140 ±0.5^b	167 ±0.1^a	168 ±0.4^a	28 ±0.1^b	85 ±0.8^b
AP_{pH12}-CS_{OSA}	141 ±0.3^b	168 ±0.6^a	169 ±0.3^a	28 ±0.6^b	89 ±0.3^c
AP_{pH12US}-CS_{OSA}	135 ±1.1^a	167 ±0.3^a	169 ±0.4^a	34 ±1.1^c	85 ±0.4^b
Treatment	Retrogradation				
	T_o, °C	T_p, °C	T_c, °C	ΔT, °C	ΔH_{gel}, j/g^{-1}
AP_N-CS_{OSA}	140 ±1.8^{ab}	167 ±0.3^a	169 ±0.3^a	28 ±1.3^b	51 ±0.8^d
AP_{US}-CS_{OSA}	141 ±0.5^{ab}	167 ±0.3^a	169 ±0.2^a	28 ±1.5^b	39 ±0.42^b
AP_{pH12}-CS_{OSA}	151 ±0.3^c	168 ±1.4^a	169 ±0.3^a	18 ±1.1^a	46 ±0.31^c
AP_{pH12US}-CS_{OSA}	136 ±1.2^a	168 ±1.3^a	169 ±0.3^a	33 ±2.1^c	36 ±0.14^a

Values are presented as mean ±SD of triplicates. Different letters in the same column indicate significant differences ($p \leq 0.05$) between means. AP_N-CS_{OSA}, AP_{US}-CS_{OSA}, AP_{pH12}-CS_{OSA}, and AP_{pH12US}-CS_{OSA} insoluble complex coacervates of native (AP_N) and modified (AP_{US}, AP_{pH12} and AP_{pH12US}) amaranth protein using ultrasonication, pH shifting and dual modification, respectively, with octenyl succinic anhydride-modified corn starch (CS_{OSA}).

increase in enthalpy may indicate greater protein denaturation, which leads to the disruption of hydrogen bonds between protein and water, forming new protein-water bonds. Additionally, a very high ΔH_{gel} suggests a higher molecular order or more stable crystals.

Starch retrogradation was analyzed 7 days after ICC formation. The T_o-R of the ICC did not show significant differences ($p \leq 0.05$) between AP_N-CS_{OSA}, AP_{US}-CS_{OSA} and AP_{pH12US}-CS_{OSA}. The highest T_o-R value (151 ±0.3°C) was observed in AP_{pH12}-CS_{OSA}. Similar to the gelatinization process, the T_p-R and T_c-R of the different ICCs did not show significant differences ($p \leq 0.05$). The range of ΔT_{ret} was statistically the same ($p \leq 0.05$) in AP_N-CS_{OSA} and AP_{US}-CS_{OSA}. The ΔH_{ret} presented significant differences ($p \leq 0.05$), with AP_N-CS_{OSA} exhibiting higher values, while the lowest ΔH_{ret} was observed in AP_{pH12US}-CS_{OSA}. The lower ΔH_{ret} values may reflect the depolymerization capacity of the microcrystals formed by the association between adjacent double helices during storage, suggesting that retrogradation of starch requires less energy to depolymerize. The % R presented values ranged from 63 ±1.1 to 43 ±0.4%. This decrease in % R can be attributed to a weaker and lower crystallinity index in retrograded starch.

Morphological properties

AP_N-CS_{OSA} (Fig. 6a) exhibits a highly porous structure, with porosity decreasing for AP_{pH12}-CS_{OSA} (Fig. 6c) and AP_{pH12US}-CS_{OSA} (Fig. 6d). This behavior

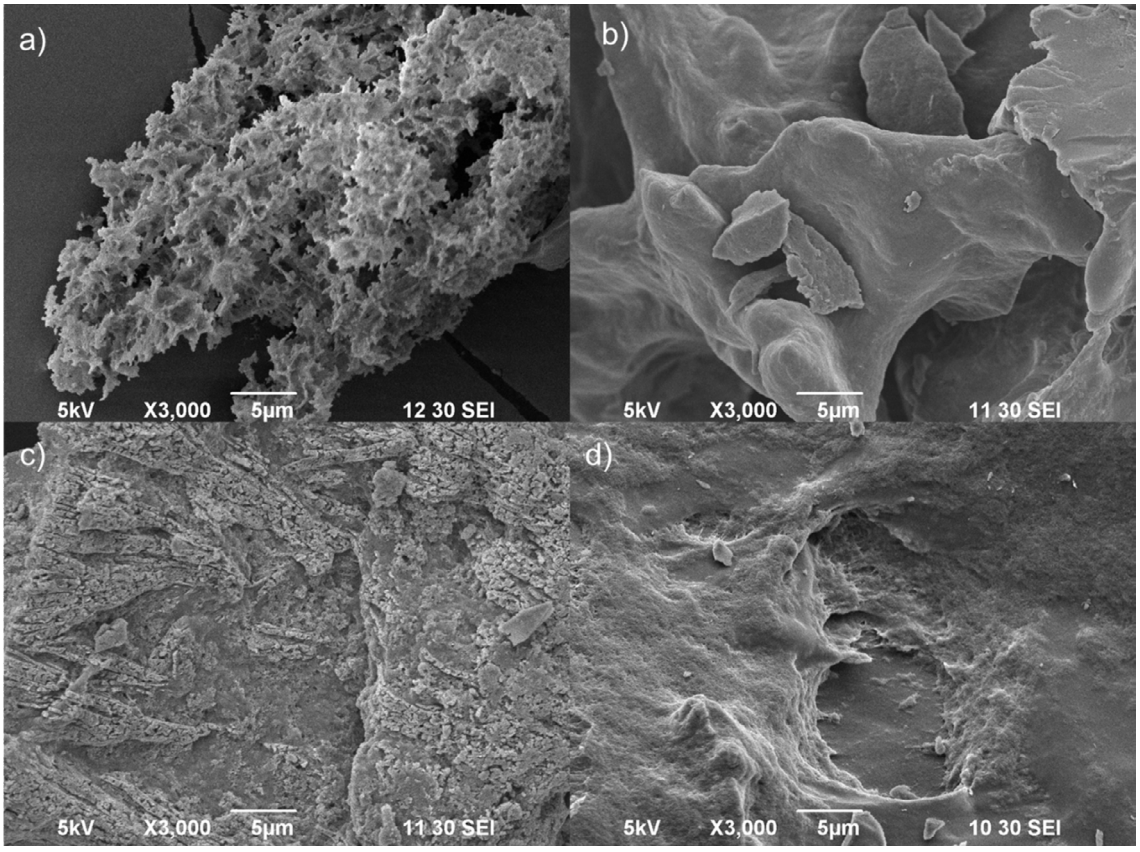

a) AP_N-CS_{OSA}, b) AP_{US}-CS_{OSA}, c) AP_{pH12}-CS_{OSA}, d) AP_{pH12US}-CS_{OSA}

Fig. 6. Scanning electron microscopy (SEM) images of insoluble complex coacervates of native (AP_N) and modified (AP_{US}, AP_{pH12} and AP_{pH12US}) amaranth proteins using ultrasonication, pH shifting and dual modification respectively, with gelatinized octenyl succinic anhydride-modified corn starch (CS_{OSA})

aligns with that reported by Li et al. (2022) in mixtures of protein (laccase and tyrosinase) and potato starch. Moreover, the porous structures suggest that the starch was completely gelatinized. In AP_{US}-CS_{OSA} (Fig. 6b), very ordered fragments with compact structures and irregularly shaped surfaces were observed; this behavior was also seen in corn starch-lutein compounds. The compact structure is attributed to starch retrogradation, a complex process involving a series of molecular rearrangements and associations.

SH and SS groups

Sulfhydryl groups are related to the formation of protein aggregates and the degree of protein denaturation. Free sulfhydryl groups (SH_f), total sulfhydryl groups (SH_t) and disulfide bonds (SS) are shown in Figure 7. The SH_f in AP_N-CS_{OSA} (2.4 µmol/g protein) increased to 2.7, 2.8 and 3.5 µmol/g protein in AP_{US}-CS_{OSA}, AP_{pH12US}-CS_{OSA} and AP_{pH12}-CS_{OSA}, respectively. Heat-treated proteins typically exhibit a higher number of free thiol groups, which are associated with the formation of protein aggregates. However, polysaccharides can activate sulfhydryl functional groups in proteins, induce new intermolecular disulfide bond bridges, and facilitate the formation of gel networks. Furthermore, the increase in SH_f is further enhanced by dual pH/ultrasonication treatments combined with thermal treatment.

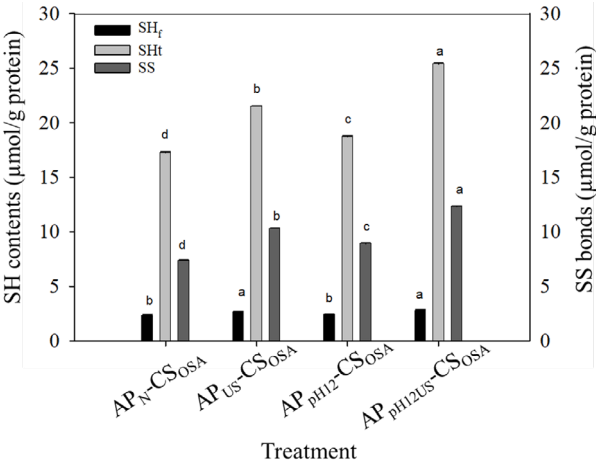

Fig. 7. Content of sulfhydryl groups (SH) and disulfide bonds (SS) in insoluble complex coacervates of native (AP_N) and modified (AP_{US}, AP_{pH12} and AP_{pH12US}) amaranth proteins using ultrasonication, pH shifting and dual modification, respectively, with octenyl succinic anhydride-modified corn starch (CS_{OSA}). The vertical bars represent the SD

The total sulfhydryl groups (SH_t) varied significantly among the ICCs. The SHt values were 25.4 ±0.12, 21.5 ±0.03, 18.7 ±0.08 and 17.2 ±0.10 µmol/g protein for AP_{pH12US}-CS_{OSA}, AP_{US}-CS_{OSA}, AP_{pH12}-CS_{OSA} and AP_N-CS_{OSA}, respectively. This increase in SH_t is likely due to the greater unfolding of the protein structure, which exposes the hydrophobic region through the US treatment, and the dual pH shift/US treatment.

Disulfide (SS) bonds increased from 7.4 ±0.2 for AP_N-CS_{OSA} to 8.1 ±0.1 µmol/g protein in AP_{pH12}-CS_{OSA}, and further increased to 10.3 ±0.3 and 12.3 ±0.1 µmol/g protein in AP_{US}-CS_{OSA} and AP_{pH12US}-CS_{OSA}, respectively. This may be attributed to the greater oxidation of the SH groups to SS bonds in the amaranth protein, which was heated and pre-treated with US and pH shift/US, then complexed with CS_{OSA}. Corn proteins have relatively low concentrations (3.8–6.2 µmol/g protein) of SS bonds (Žilić et al., 2012), suggesting that when corn starch is modified with OSA (3%) and complexed with heated amaranth protein modified by pH shifting, US, and dual treatments (pH shifting/ US), the SS bonds increase substantially.

Thus, the SS content in the different ICCs contributes to better-sticking properties during gelatinization, as shown in Table 5. Disulfide bonds are formed by the oxidation of sulfhydryl groups. At high alkaline pH, SH_f groups on protein molecules are exposed due to partial unfolding of the protein structure. Therefore, at alkaline pH, the exposed and activated SH groups of protein molecules can be oxidized by the highly reactive free radicals generated by ultrasound, leading to the formation of intermolecular disulfide bridges (Alavi et al., 2021). Furthermore, heating the protein solution causes buried SH groups to be exposed, resulting in an increase in the thiol content. In polysaccharide-whey protein isolated complexes, two opposing factors can affect the free thiol content: (a) the steric hindrance caused by the polysaccharide, which restricts access to the free SH groups and (b) prevention of whey protein S-S bond formation by the polysaccharide during heat treatment (Zamani et al., 2020).

CONCLUSIONS

Vegetable by-products, such as proteins and starches, can be utilized in the formation of ICCs. However, they must first be modified using chemical and physical techniques to enhance their techno-functional properties and digestibility. The pH shift and/or combination with ultrasound (US) had significant effects on modifying the protein structure and the starch bands present in the different ICCs. These changes, in turn, affected the digestibility of both the protein and starch. The percentage of resistant starch present in the different ICCs suggests that these complexes have excellent potential for use in food formulations. ICCs formulated with amaranth protein (AP) modified by pH shift, US or the dual combination of pH shifting/US exhibited a decrease in starch retrogradation when complexed with AP.

In general, amaranth protein and corn starch can be effectively used in various food processes, and their complexation can be further enhanced using environmentally friendly technologies. Therefore, this study contributes by providing low-cost and accessible methodologies for modifying biopolymers (amaranth protein and corn starch), thus improving their techno-functional properties, structure and digestibility for the formulation of insoluble complex coacervates. Furthermore, the knowledge gained from this work could expand the application of ICCs in the development and production of functional foods.

ACKNOWLEDGEMENTS

Author (J.J.F.G.) thanks the Consejo Nacional de Humanidades, Ciencia y Tecnología de México (CONAHCyT) for his Ph. D. scholarship.

DECLARATIONS

Data statement
All data supporting this study has been included in this manuscript.

Ethical Approval
Not applicable.

Competing Interests
The authors declare that they have no conflicts of interest.

REFERENCES

Alavi, F., Chen, L., Emam-Djomeh, Z. (2021). Effect of ultrasound-assisted alkaline treatment on functional property modifications of faba bean protein. Food Chem., 354, 129494. https://doi.org/10.1016/j.foodchem.2021.129494

AOAC (1996). Official methods of analysis of AOAC international (16th Ed). Rockville, MD: AOAC International.

Bai, M., Qin, G., Sun, Z., Long, G. (2016). Relationship between molecular structure characteristics of feed proteins and protein *in vitro* digestibility and solubility. Asian-Australas. J. Anim. Sci., 29(8), 1159–1165. https://doi.org/10.5713/ajas.15.0701

Carbonaro, M., Maselli, P., Nucara, A. (2012). Relationship between digestibility and secondary structure of raw and thermally treated legume proteins: a Fourier transform infrared (FT-IR) spectroscopic study. Amino Acids, 43(2), 911–921. https://doi.org/10.1007/s00726-011-1151-4

Carbonaro, M., Maselli, P., Nucara, A. (2015). Structural aspects of legume proteins and nutraceutical properties. Food Res. Int., 76, 19-30. https://doi.org/10.1016/j.foodres.2014.11.007

Cuevas-Bernardino, J. C., Leyva-Gutierrez, F. M., Vernon-Carter, E. J., Lobato-Calleros, C., Román-Guerrero, A., Davidov-Pardo, G. (2018). Formation of biopolymer complexes composed of pea protein and mesquite gum–Impact of quercetin addition on their physical and

chemical stability. Food Hydrocoll., 77, 736–745. https://doi.org/10.1016/j.foodhyd.2017.11.015

Espinosa-Andrews, H., Lobato-Calleros, C., Loeza-Corte, J. M., Beristain, C. I., Rodríguez-Huezo, M. E., Vernon-Carter, E. J. (2008). Quantification of the composition of gum arabic-chitosan coacervates by HPLC. Rev. Mex. Ing. Quím., 7, 293–298. https://www.scielo.org.mx/scielo.php?script=sci_arttext&pid=S1665-27382008000300014

Feng, Y. Y., Mu, T. H., Zhang, M., Ma, M. M. (2020). Effects of ionic polysaccharides and egg white protein complex formulations on dough rheological properties, structure formation and *in vitro* starch digestibility of wet sweet potato vermicelli. Int. J. Biol. Macromol., 149, 1170–1179. https://doi.org/10.1016/j.ijbiomac.2020.02.020

Figueroa-González, J. J., Lobato-Calleros, C., Vernon-Carter, E. J., Aguirre-Mandujano, E., Alvarez-Ramirez, J., Martínez-Velasco, A. (2022). Modifying the structure, physicochemical properties, and foaming ability of amaranth protein by dual pH-shifting and ultrasound treatments. LWT, 153, 112561. https://doi.org/10.1016/j.lwt.2021.112561

Flores-Silva, P., Martínez-Yañez, R. C., Rodríguez-Huezo, M. E., Alvarez-Ramirez, J. (2022). Nutritional protein quality and digestibility changes during food processing. Rev. Mex. Ing. Quím., 21(1), Alim2748. https://doi.org/10.24275/rmiq/Alim2748

García-de la Rosa, K., Lobato-Calleros, C., Hernández-Rodríguez, L., Aguirre-Mandujano, E. (2023). Rheological and structural properties of complex coacervates of *Amaranthus hypochondriacus* protein-citrus pectin. Rev. Mex. Ing. Quim., 22(1), Alim3003. https://doi.org/10.24275/rmiq/Alim3003

Hsu, H. W., Vavak, D. L., Satterlee, L., Miller, G. A. (1977). A multienzyme technique for estimating protein digestibility. J. Food Sci., 42, 1269–1273. https://doi.org/10.1111/j.1365-2621.1977.tb14476.x

Jones, O. G., Decker, E. A., McClements, D. J. (2009). Formation of biopolymer particles by thermal treatment of β-lactoglobulin–pectin complexes. Food Hydrocoll., 23, 1312–1321. https://doi.org/10.1016/j.foodhyd.2008.11.013

Kamani, M. H., Semwal, J., Khaneghah, A. M. (2022). Functional modification of grain proteins by dual approaches: Current progress, challenges, and future perspectives. Colloids Surf. B Biointerfaces, 211, 112306. https://doi.org/10.1016/j.colsurfb.2021.112306

Lee, Y. K., Chang, Y. H. (2019). Structural and *in vitro* digestibility properties of esterified maca starch with citric acid and its application as an oil-in-water (O/W) pickering emulsion stabilizer. Int. J. Biol. Macromol., 134, 798–806. https://doi.org/10.1016/j.ijbiomac.2019.05.081

Li, Y., Cheng, Y., Zhang, Z., Wang, Y., Mintah, B. K., Dabbour, M., Jiang, H., He, R., Ma, H. (2020). Modification of rapeseed protein by ultrasound-assisted pH shift treatment: Ultrasonic mode and frequency screening, changes in protein solubility and structural characteristics. Ultrason. Sonochem., 69, 105240. https://doi.org/10.1016/j.ultsonch.2020.105240

Li, Y., Li, R., Chen, S., Wang, X., Jiang, Y., Fang, Y., Lin, Q., Ding, Y. (2024). Understanding regulating effects of protein-anionic octenyl succinic anhydride-modified starch interactions on the structural, rheological, digestibility and release properties of starch. J. Sci. Food Agric., 104(4), 8580–8592. https://doi.org/10.1002/jsfa.13686

Lin, D., Lu, W., Kelly, A. L., Zhang, L., Zheng, B., Miao, S. (2017). Interactions of vegetable proteins with other polymers: Structure-function relationships and applications in the food industry. Trends Food Sci. Technol., 68, 130–144. https://doi.org/10.1016/j.tifs.2017.08.006

Lopez-Silva, M., Bello-Perez, L. A., Agama-Acevedo, E., Alvarez-Ramirez, J. (2019). Effect of amylose content in morphological, functional and emulsification properties of OSA modified cornstarch. Food Hydrocoll., 97, 105212. https://doi.org/10.1016/j.foodhyd.2019.105212

Mejía-Terán, A., Blanco-Tizarazo, C. M. (2021). Considerations for functional food design based on starch-protein interactions: a systematic review. Int. J. Food Sci. Nutr., 72, 1009–1018. https://doi.org/10.1080/09637486.2021.1905784

Mendez-Montealvo, G., Wanga, Y-J., Campbell, M. (2011). Thermal and rheological properties of granular waxy maize mutant starches after β-amylase modification. Carbohydr. Polym., 83, 1106–1111. https://doi.org/10.1016/j.carbpol.2010.09.012

Miller, G. L. (1959). Use of dinitrosalicylic acid reagent for determination of reducing sugar. Anal. Chem., 31(3), 426–428. https://doi.org/10.1021/ac60147a030

Mir, N. A., Riar, C. S., Singh, S. (2019). Structural modification of quinoa seed protein isolates (QPIs) by variable time sonification for improving its physicochemical and functional characteristics. Ultrason. Sonochem., 58, 104700. https://doi.org/10.1016/j.ultsonch.2019.104700

Nazari, B., Mohammadifar, M. A., Shojaee-Aliabadi, S., Feizollahi, E., Mirmoghtadaie, L. (2018). Effect of ultrasound treatments on functional properties and structure of millet protein concentrate. Ultrason. Sonochem., 41, 382–388. https://doi.org/10.1016/j.ultsonch.2017.10.002

Nissen, S. H., Schmidt, J. M., Gregersen, S., Hammershøj, M., Møller, A. H., Danielsen, M., Dalsgaard, T. K. (2021). Increased solubility and functional properties of precipitated alfalfa protein concentrate subjected to pH shift processes. Food Hydrocoll., 119, 106874. https://doi.org/10.1016/j.foodhyd.2021.106874

Paredes-López, O. (2018). Amaranth Biology, Chemistry and Technology. Boca Raton, Florida, USA: CRC Press.

Park, I-M., Ibáñez, A. M., Zhong, F., Shoemaker, E. F. (2007). Gelatinization and pasting properties of waxy and non-waxy rice starches. Starch-Stärke, 59, 388–396. https://doi.org/10.1002/star.200600570

Rodríguez-Rodríguez, R., Espinosa-Andrews, H., Morales-Hernández, N., Lobato-Calleros, C., Vernon-Carter, E. J. (2018). Mesquite gum/chitosan insoluble complexes: relationship between the water state and viscoelastic properties. J. Disper. Sci. Technol., 40, 1345–1352. https://doi.org/10.1080/01932691.2018.1513848

Rothenbuhler, E., Kinsella, J. E. (1985). The pH-Stat method for assessing protein digestibility: an evaluation. J. Agricult. Food Chem., 33(3), 433–438. https://doi.org/10.1021/jf00063a027

Wang, Z., Fan, M., Hannachi, K., Li, Y., Qian, H., Wang, L. (2023). Impact of red kidney bean protein on starch digestion and exploring its underlying mechanism. Int. J. Biol. Macromol., 253, 127023. https://doi.org/10.1016/j.ijbiomac.2023.127023

Wu, D., Lin, Q., Singh, H., Ye, A. (2020). Complexation between whey protein and octenyl succinic anhydride (OSA)-modified starch: Formation and characteristics of soluble complexes. Food Res. Int., 136, 109350. https://doi.org/10.1016/j.foodres.2020.109350

Xu, T., Jiang, C., Zhou, Q., Gu, Z., Cheng, L., Tong, Y., Hong, Y. (2021). Preparation and characterization of octenyl succinic anhydride modified waxy maize starch hydrolyzate/chitosan complexes with enhanced interfacial properties. Carbohydr. Polym., 267, 118228. https://doi.org/10.1016/j.carbpol.2021.118228

Yang, J., Dou, J., Zhu, B., Ning, Y., Wang, H., Huang, Y., Jiang, L. (2023). Multi-dimensional analysis of heat-induced soybean protein hydrolysate gels subjected to ultrasound-assisted pH pretreatment. Ultrason. Sonochem., 95, 106403. https://doi.org/10.1016/j.ultsonch.2023.106403

Yang, J., Duan, Y., Geng, F., Cheng, C., Wang, L., Ye, J., Deng, Q. (2022). Ultrasonic-assisted pH shift-induced interfacial remodeling for enhancing the emulsifying and foaming properties of perilla protein isolate. Ultrason. Sonochem., 89, 106108. https://doi.org/10.1016/j.ultsonch.2022.106108

Yang, Y., He, S., Ye, Y., Cao, X., Liu, H., Wu, Z., Yue, J., Sun, H. (2020). Enhanced hydrophobicity of soybean protein isolate by low-pH shifting treatment for the submicron gel particles preparation. Ind. Crops Prod., 151, 112475. https://doi.org/10.1016/j.indcrop.2020.112475

Yang, W., Kong, X., Zheng, Y., Sun, W., Chen, S., Liu, D., Ye, X. (2019). Controlled ultrasound treatments modify the morphology and physical properties of rice starch rather than the fine structure. Ultrason. Sonochem., 59, 104709. https://doi.org/10.1016/j.ultsonch.2019.104709

Ye, J., Luo, S., Huang, A., Chen, J., Liu, C., McClements, D. J. (2019). Synthesis and characterization of citric acid esterified rice starch by reactive extrusion: A new method of producing resistant starch. Food Hydrocoll., 92, 135–142. https://doi.org/10.1016/j.foodhyd.2019.01.064

Zamani, H., Zamani, S., Zhang, Z., Abbaspourrad, A. (2020). Exceptional colloidal stability of acidified whey protein beverages stabilized by soybean soluble polysaccharide. J. Food Sci., 85(4), 989–997. https://doi.org/10.1111/1750-3841.15041

Zhang, T., Zhao, Y., Tian, X., Liu, J., Ye, H., Shen, X. (2021a). Effect of ultrasound pretreatment on structural, physicochemical, rheological and gelation properties of transglutaminase cross-linked whey protein soluble aggregates. Ultrason. Sonochem., 74, 105553. https://doi.org/10.1016/j.ultsonch.2021.105553

Zhang, W., Liu, C., Zhao, J., Ma, T., He, Z., Huang, M., Wang, Y. (2021b). Modification of structure and functionalities of ginkgo seed proteins by pH-shifting treatment. Food Chem., 358, 129862. https://doi.org/10.1016/j.foodchem.2021.129862

Žilić, S., Akıllıoğlu, G., Serpen, A., Barać, M., Gökmen, V. (2012). Effects of isolation, enzymatic hydrolysis, heating, hydratation and Maillard reaction on the antioxidant capacity of cereal and legume proteins. Food Res. Int., 49, 1–6. https://doi.org/10.1016/j.foodres.2012.06.031